AFRL-AFOSR-JP-TR-2023

Investigation into an optimum device structure for cladding light removal in high power fiber lasers

Ju Han Lee
University of seoul industry cooperation foundation
163 Seoulsiripdae-ro
Dongdaemun-gu, Seoul,, , 02504
KR

11/19/2022
Final Technical Report

Air Force Research Laboratory
Air Force Office of Scientific Research
Asian Office of Aerospace Research and Development
Unit 45002, APO AP 96338-5002

REPORT DOCUMENTATION PAGE

PLEASE DO NOT RETURN YOUR FORM TO THE ABOVE ORGANIZATION.

1. REPORT DATE	2. REPORT TYPE	3. DATES COVERED	
20221119	Final	START DATE 20200930	END DATE 20220929

4. TITLE AND SUBTITLE
Investigation into an optimum device structure for cladding light removal in high power fiber lasers

5a. CONTRACT NUMBER	5b. GRANT NUMBER	5c. PROGRAM ELEMENT NUMBER
	FA2386-20-1-4055	
5d. PROJECT NUMBER	**5e. TASK NUMBER**	**5f. WORK UNIT NUMBER**

6. AUTHOR(S)
Ju Han Lee

7. PERFORMING ORGANIZATION NAME(S) AND ADDRESS(ES)
University of seoul industry cooperation foundation
163 Seoulsiripdae-ro
Dongdaemun-gu, Seoul, 02504
KR

8. PERFORMING ORGANIZATION REPORT NUMBER

9. SPONSORING/MONITORING AGENCY NAME(S) AND ADDRESS(ES)	10. SPONSOR/MONITOR'S ACRONYM(S)	11. SPONSOR/MONITOR'S REPORT NUMBER(S)
AOARD UNIT 45002 APO AP 96338-5002	AFRL/AFOSR IOA	AFRL-AFOSR-JP-TR-2023-0045

12. DISTRIBUTION/AVAILABILITY STATEMENT
A Distribution Unlimited: PB Public Release

13. SUPPLEMENTARY NOTES

14. ABSTRACT
In this work, we systematically investigated backward scattering within a cladding light stripper based on a periodically grooved structure of an optical fiber, to figure out the method for its efficient suppression through numerical simulation. On the basis of the investigation results a novel, periodically grooved CLS structure that allows for efficient suppression of backward scattering of cladding light, was thus proposed. More specifically, the relationship between backward scattering of cladding light and the cladding surface roughness of a periodically-grooved CLS was investigated using the ray tracing method. It was shown that the amount of backward scattering of cladding light is dependent on the groove surface roughness and the undesired backward scattering significantly affects the cladding light tripping capability of a CLS. As a result of this theoretical investigation, a periodically-grooved CLS structure with multiple no groove sections of proper length was proposed and its efficacy was then verified through a numerical simulation and an experiment.

15. SUBJECT TERMS

16. SECURITY CLASSIFICATION OF:			17. LIMITATION OF ABSTRACT	18. NUMBER OF PAGES
a. REPORT U	b. ABSTRACT U	c. THIS PAGE U	SAR	18

19a. NAME OF RESPONSIBLE PERSON	19b. PHONE NUMBER *(Include area code)*
TONY KIM	315-227-7008

Progress Report - Final

- Award number for this report: FA2386-20-1-4055
- Proposal Title: Investigation into an optimum device structure for cladding light removal in high power fiber lasers
- Principle Investigator: Ju Han Lee (Professor)
- Key Researcher(s) involved in the Proposed Project: Tae Yoon Kim, Geun Won Lim
- Affiliation of each Researcher(s): University of Seoul, School of Electrical and Computer Engineering, 163 Seoulsiripdae-ro, Dongdaemun-gu, Seoul, 02504, South Korea

Research Objectives:

- The main goal of this project is to find the optimum structure of a CLS, which can be used for future high power fiber lasers. In this two-year research project, we propose to explore various CLS structures and to find an optimum structure with the features of a high power handling capacity, a large cladding loss, and uniform light extraction with no hot spot issue. We plan to theoretically investigate CLS structures by solving beam propagation modes within the device with a numerical simulation technique. In particular, both backward scattering and forward scattering are to be taken into account. One of the main focuses in our investigation is to design a repeatable and reliable device structure in terms of easy and repeatable fabrication rather than to simply use roughened surface structures.
- In the first year of the project, we will focus on the theoretical understanding and design aspects of CLS's. In this stage, the main focus of our research will be placed on a full-understanding of backward scattering and forward scattering under various CLS structures. In the second year, an optimum CLS structure will be designed and its efficacy will then be verified with numerical simulation results.
- Our yearly research objectives are summarized below.

Research Objectives	**Percentage of completion**
• Theoretical understanding of design aspects of CLS's	100%
• Full-understanding of backward scattering and forward scattering under various CLS structures	100%
• Design of an optimum CLS structure	100%
• Theoretical performance evaluation	100%

- **Details of accomplishments during this reporting period.**

In this work, we systematically investigated backward scattering within a cladding light stripper based on a periodically grooved structure of an optical fiber, to figure out the method for its efficient suppression through numerical simulation. On the basis of the investigation results a novel, periodically grooved CLS structure that allows for efficient suppression of backward scattering of cladding light, was thus proposed. More specifically, the relationship between backward scattering of cladding light and the cladding surface roughness of a periodically-grooved CLS was investigated using the ray tracing method. It was shown that the amount of backward scattering of cladding light is dependent on the groove surface roughness and the undesired backward scattering significantly affects the cladding light stripping capability of a CLS. As a result of this theoretical investigation, a periodically-grooved CLS structure with multiple no-groove sections of proper length was proposed and its efficacy was then verified through a numerical simulation and an experiment.

1. Theoretical analysis

Fig. 1 presents the definition of the parameters ω_r, f_r, θ , and φ for the geometry of the incident and reflected light used in this theoretical investigation. In order to investigate the scattering of the cladding light on the rough surface of the periodic grooves, we use commercially available ray-tracing software (Matlab, Lumerical). In this ray-tracing algorithm, the surface is divided into many regular interval points. The characteristics of the lightwaves propagated at each point on the surface are governed by both Snell's law and Fresnel's equation. After the scattering of the lightwaves on the rough surface, the scattered beams are assumed to propagate with various amplitudes in a direction that differs from that of the incident beam. Note that the ray-tracing method is believed to be applied only to CLSs based on the wet etching method, since the roughness level of the etched surface is much larger than the wavelength of propagating light in these types of CLSs. However, the ray-tracing method would not be appropriate for performance analysis of CLSs based on CO_2 laser processing, which exhibits a surface roughness level of micrometers or below.

1.1 Bidirectional reflection

When light is incident to a point on the rough surface, the energy of the lightwaves can be absorbed, transmitted, or reflected. The bidirectional reflection distribution function (BRDF) can be used to calculate the angular distribution of the lightwave radiance [23, 24] Using the BRDF, the lightwave reflection characteristics of the rough surface of a grooved section can be expressed as

$$f_r(\theta_i, \phi_i; \theta_r, \phi_r) = dL_r(\theta_i, \phi_i; \theta_r, \phi_r; E_i) / dE_i(\theta_i, \phi_i) \qquad (1)$$

where f_r is the bidirectional reflectance distribution function, and θ and φ denote the polar angle and azimuthal angle, respectively. The subscripts i and r denote the incidence and reflection of the flux radiance. E_i is the incident irradiance. During the simulation process, we assume that f_r is constant over all solid angles ω_r.

1.2 Surface roughness

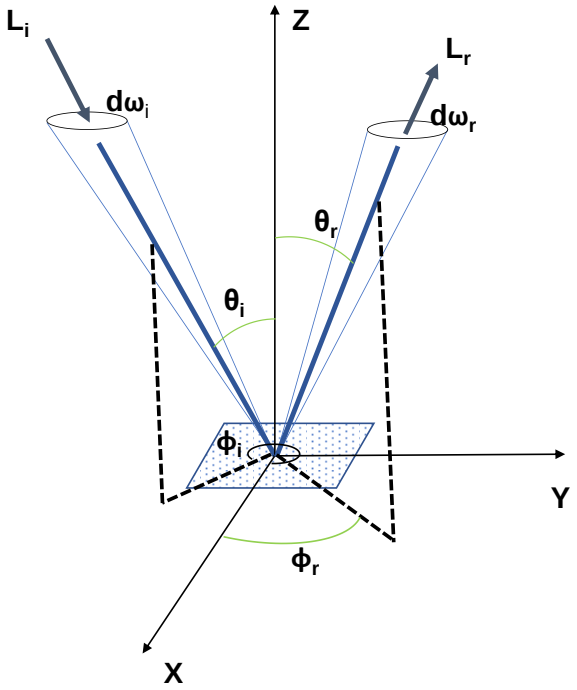

Fig. 1. Definition of parameters ω_r, f_r, θ, and φ in the geometry of incident and reflected light.

The properties of a randomly rough surface can be described with both an autocovariance function and a height distribution function [24]. The former describes the lateral distribution of the surface peaks and valleys, while the latter reflects the deviation from the mean surface height. The height distribution $P_h(\xi)$ and autocovariance functions $C(x,y)$ are given by Gaussian functions [24]:

$$p_h(\xi) = \frac{1}{\sqrt{2\pi\sigma^2}} \exp\left(-\frac{\xi^2}{2\sigma^2}\right) \tag{2}$$

$$C(x,y) = \exp\left(-\frac{x^2}{\gamma_x^2} - \frac{y^2}{\gamma_y^2}\right) \tag{3}$$

where σ indicates the root-mean-square (*rms*) height of the randomly rough surface. γ_x and γ_y denote the correlation lengths of the *x*- and *y*-axis, respectively. The correlation length indicates the maximum distance, which yields a reasonable estimate of the heights of neighboring points [23, 24]. For our calculation we used a fixed correlation length of 1 μm, which was obtained from Ref. [23]. Because the surface is assumed to be isotropic, there is no preferential roughness direction ($\gamma_x = \gamma_y = \gamma$). The mean local slope of the surface is given by $\sqrt{2}\sigma/\gamma$, and $\sqrt{2}$ can be eliminated to simplify the slope factor. The ratio of σ/γ thus represents the mean local slope of the surface.

1.3 Geometric Approximation

Geometric approximation, which is also referred to as ray tracing, is a technique that traces the energy flow of a lightwave until it leaves the surface [25]. It provides information on the

effect of the surface roughness on lightwave scattering behavior. In this calculation, a scattering point is selected by comparing the tangent angle of the point relative to the angle of the incidence ray. Snell's law and the Fresnel equation are applied to the non-shadowed points of the surface [23, 24].

2. Simulation results

In this investigation, the incidence angle (θ_i) and reflection angle (θ_r) on the rough surface are defined as shown in Fig. 2. Fig. 3 illustrates the light intensity distribution as a function of the reflection angle for various mean local slopes (σ/γ) in the extreme case where the incidence angle on the rough surface of the silica fiber is 0˚. Different values for σ/γ reflect differences in the roughness of the surface. These results are obtained by averaging the values obtained after 10,000 iterations.

For σ/γ = 0.01, which reflects a very low fiber surface roughness, light reflection mainly occurs at a reflection angle (θ_r) of 0˚. When the mean local slope is increased to σ/γ = 0.1, light reflection starts to occur at a slightly wider range of reflection angles. With a further increase in σ/γ (σ/γ = 2), the reflection angle distribution becomes broader and lightwave reflection is observed to occur at almost all reflection angles.

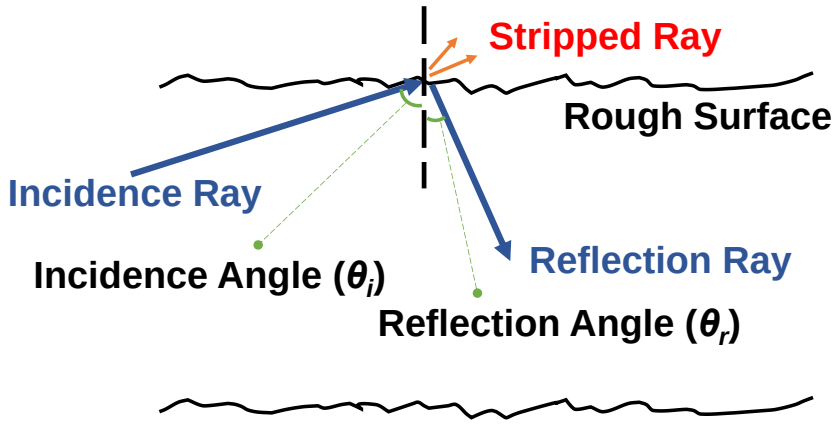

Fig. 2. Definition of the incidence angle and reflection angle for a rough surface.

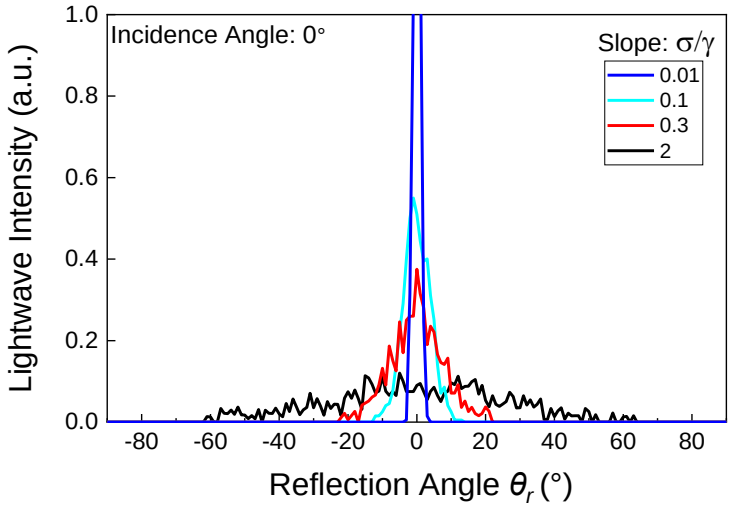

Fig. 3. Lightwave intensity distribution as a function of the reflection angle for various values of the mean local slope (σ/γ), when the incidence angle is 0˚.

As an example optical fiber, we consider the numerical aperture of a typical double-clad optical fiber with a diameter of 400 μm. It can be inferred from the numerical aperture that the incidence angle (θ_i) of the cladding lightwave propagating in the inner cladding region should be between 78.5˚and 90˚. When the lightwave arrives at a point on the rough surface, the lightwave is reflected in either the forward or backward direction depending on the local slope of the surface point. Using ray-tracing simulations, it is possible to estimate the proportion of lightwave stripped at a local point on the rough surface. The local lightwave stripping efficiency *(η)* at a single point on the rough surface can be defined as follows:

$$Lightwave\ stripping\ efficiency(\eta) = \frac{Total\ energy\ of\ \ stripped\ lightwave}{Total\ energy\ of\ \ incidence\ lightwave} \tag{4}$$

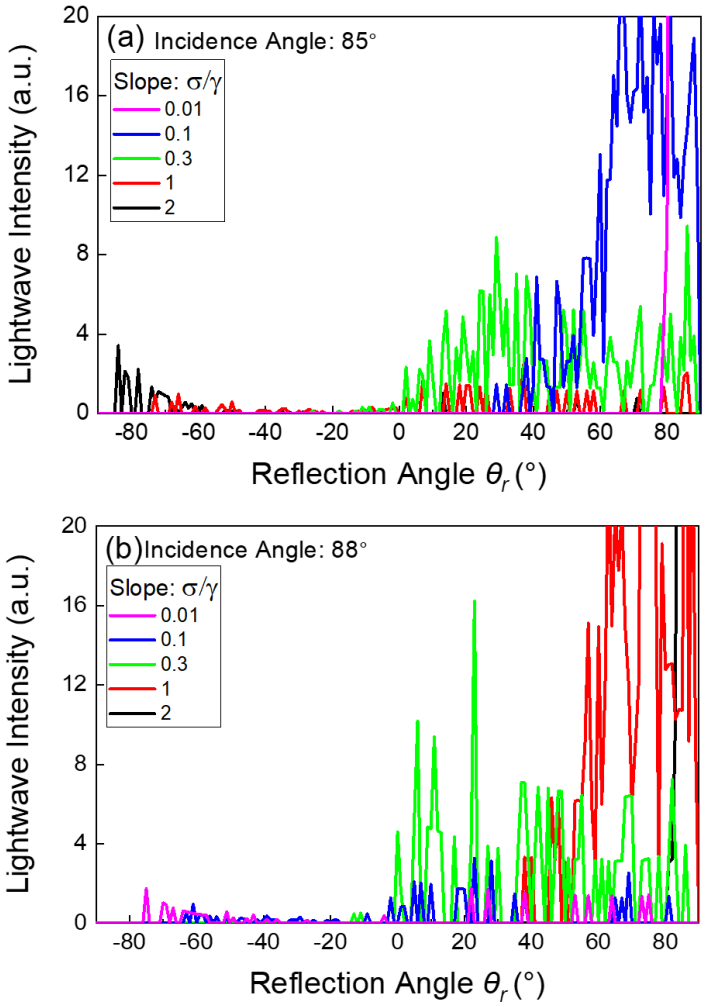

Fig. 4. Lightwave intensity distribution as a function of the reflection angle for various values of the mean local slope (σ/γ), when the incidence angle is (a) 85˚, and (b) 88˚.

Fig. 4 presents the lightwave intensity distribution as a function of the reflection angle (θ_r) for various σ/γ values and incidence angles (θ_i) of 85˚ and 88˚. When the incidence angle is 85˚, the distribution of reflected lightwave resembles a delta function for σ/γ=0.01. When the mean local slope increases to σ/γ=0.1 or σ/γ=0.3, the distribution becomes broader and the

stripping efficiency increases. The stripping efficiency increases from 0.01% to 96% as the slope increases from σ/γ=0.01 to 2. Because an increase in the σ/γ of a point on the rough surface forces lightwaves to violate the total internal reflection (TIR) condition, it can be predicted that more lightwaves can be stripped as the roughness of the fiber surface increases. It should be noted that substantial backscattered light occurs at σ/γ=2. In particular, a non-negligible number of backscattered lightwaves are present in a direction of nearly −90˚. It is well-known that backscattered lightwaves in the direction of −90˚ are detrimental for high-power fiber laser oscillators or amplifiers because they cannot be stripped away and can damage fiber laser systems. The lightwave intensity distribution as a function of the reflection angle (θ_r) for σ/γ values and an incidence angle of 88˚ is shown in Fig. 4(b). By comparing the results with those for an incidence angle of 85˚ when σ/γ is increased from 0.01 to 2, it is clear that incident lightwaves with a smaller incidence angle at a point on the rough surface generate a higher number of backscattered lightwaves.

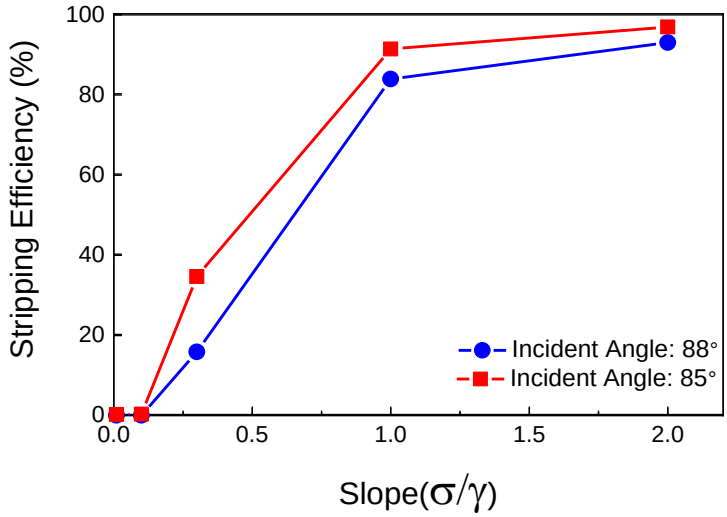

Fig. 5. Local lightwave stripping efficiency at an incidence angle (θ_i) of 85˚ and 88˚ for various values of the mean local slope (σ/γ).

2.1 Second scattered light on rough surface

In order to obtain a clearer understanding of lightwave scattering on a rough surface, we investigate secondary scattering (Fig. 6), which occurs at another point on the rough surface after the initial scattering. When secondary scattering is considered, more backscattering in the −90˚ direction is observed compared with the initial scattering only.

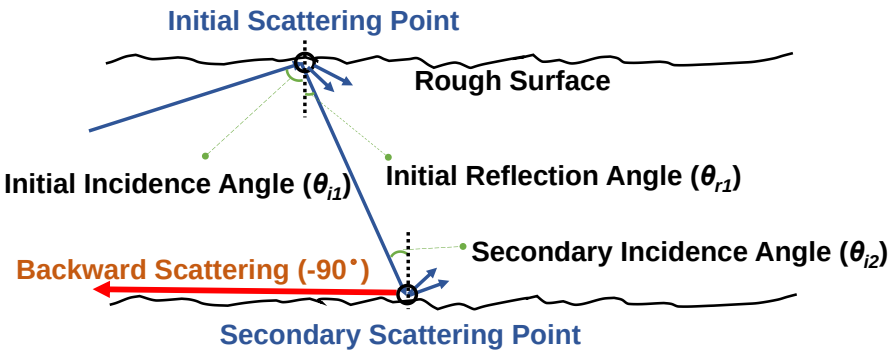

Fig. 6. Schematic diagram of initial and secondary scattering on a rough surface.

Fig. 7 presents the distribution of the lightwave intensity calculated as a function of the initial reflection angle (θ_{r1}) for the initial scattering on a rough surface with σ/γ=0.5 and an initial incidence angle (θ_{i1}) of 85˚. The intensity of the lightwaves scattered in the backward direction is only 4.2% of that of the total scattered lightwaves. This, the initial scattering does not involve significant scattering in the backward direction even though the σ/γ is high. However, when secondary scattering is accounted for, lightwaves reflected in a forward direction from the initial scattering point can be scattered backward when reflected from a second scattering point on the rough surface. Our calculations show that incident lightwaves from the first scattering point with an initial incidence angle of 0˚ to 10˚ can generate a significant number of lightwaves scattered in the backward direction when secondary scattering is factored in. Fig. 8 presents the distribution of the calculated lightwave intensity as a function of the secondary reflection angle (θ_{r2}) under various initial incidence angles θ_{i1} (10, 8, 6, and 4˚) for the lightwaves at σ/γ=0.5. Detrimental backward scattered lightwaves in the −90˚ direction are produced with all four initial incidence angles, with the levels of backward scattered light increasing as the incidence angle becomes smaller. This phenomenon is not observed when initial scattering only is considered.

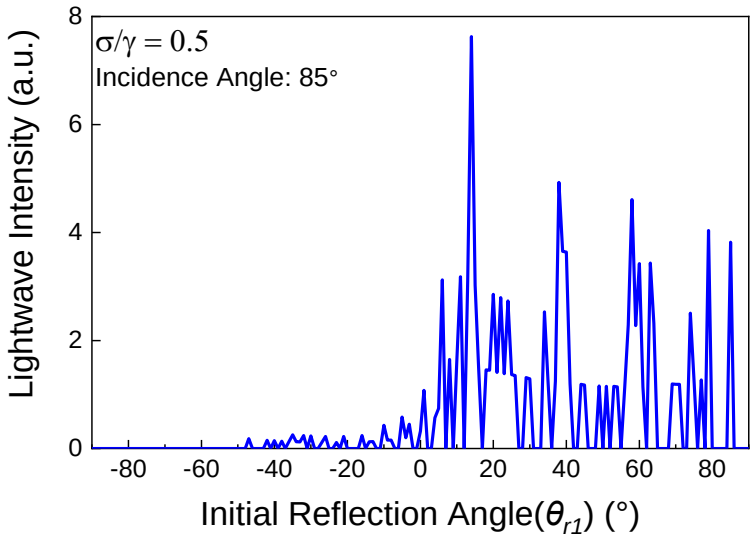

Fig. 7. Calculated lightwave intensity distribution as a function of the initial reflection angle (θ_{r1}) at the first scattering point with an initial incidence angle of 85˚ and σ/γ=0.5.

Fig. 9 displays the ratio of all backward scattered lightwaves relative to all scattered light as a function of the initial incidence angle (θ_{i1}). When θ_{i1} is smaller than 10˚, nearly 50% of the initial incident lightwaves are scattered in the backward direction. The proportion of backward scattered lightwaves abruptly decreases when θ_{i1} is higher than 20˚, particularly in the −90˚ direction.

2.2 Lightwave scattering in typical multi-section structures

As mentioned, backscattering is a critical limiting factor for CLSs, meaning that the effective suppression of backscattering is essential to improving CLS performance. The CLS structures that have been reported to date are based on the use of different levels of surface roughness or on periodically grooved sections [13, 14, 15, 16, 17]. Fig. 10 presents a representative CLS structure with periodically grooved sections with different levels of surface roughness [14, 17, 18, 20]. This structure consists of two sections: the first with a large diameter and a low surface roughness (σ/γ=0.5), and the second with a low diameter and a high surface roughness (σ/γ=1).

It is well-known that a higher surface roughness can generate more backscattering [25, 26], though it can also lead to the more effective stripping of lightwaves. In order to analyze lightwave scattering in the structure presented in Fig. 10, we assume that initial scattering occurs in the first section and secondary scattering occurs in the second section.

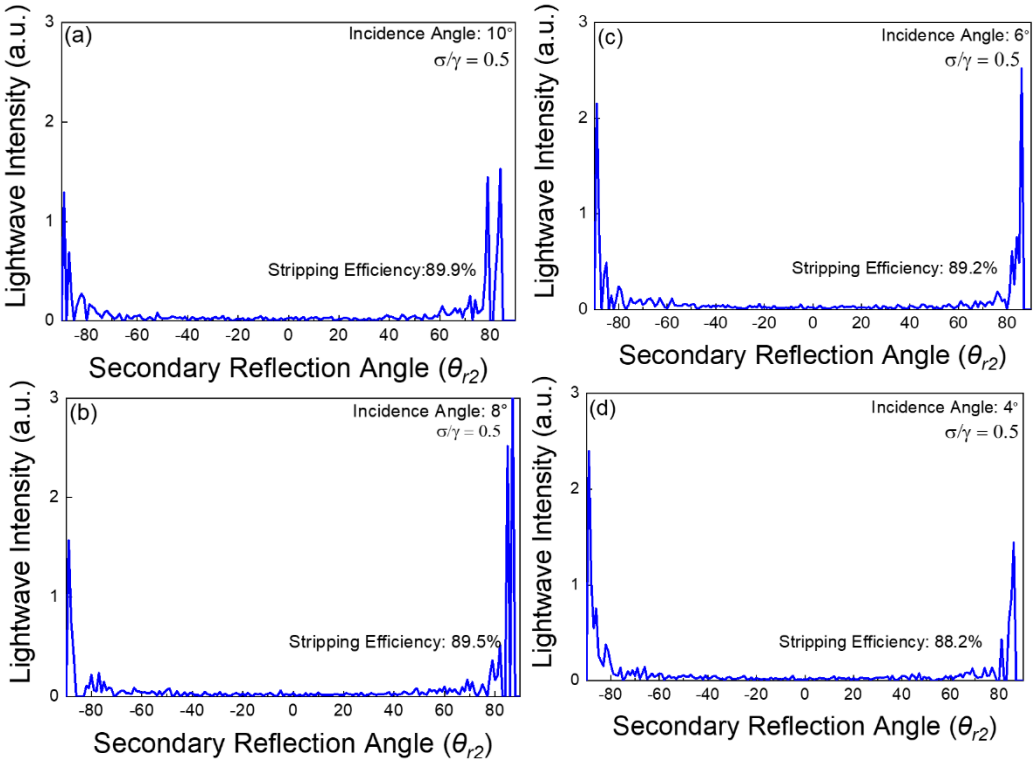

Fig. 8. Calculated lightwave intensity distribution as a function of the secondary reflection angle (θ_{r2}) with incidence angles of (a) 4˚, (b) 6˚, (c) 8˚, and (d) 10˚ at σ/γ=0.5.

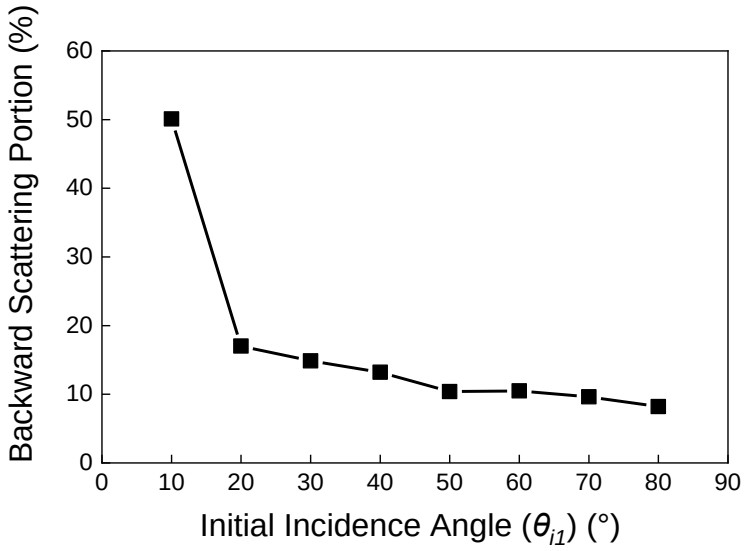

Fig. 9 Proportion of back scattered lightwaves relative to all scattered light as a function of the initial incidence angle (θ_{i1}) at σ/γ=0.5.

The distribution of the calculated lightwave intensity as a function of the initial reflection angle (θ_{r1}) for an incident angle of 85˚ is shown in Fig. 11. In this calculation, σ/γ=0.5 and 1 are considered. More backscattering occurs for σ/γ=1 than for 0.5, though the former has a

lightwave stripping efficiency of 88.6%, which is much higher than the 51.9% for the latter. However, backscattering is higher when secondary scattering in the second section is accounted for. As shown in Fig. 11(a), a significant number of lightwaves are scattered at the initial scattering point with a reflection angle range of 0°−80° and then the scattered lightwaves are scattered again at the surface with σ/γ=1 in the second section. As previously mentioned, a surface roughness level of σ/γ=1 can lead to significant backscattering.

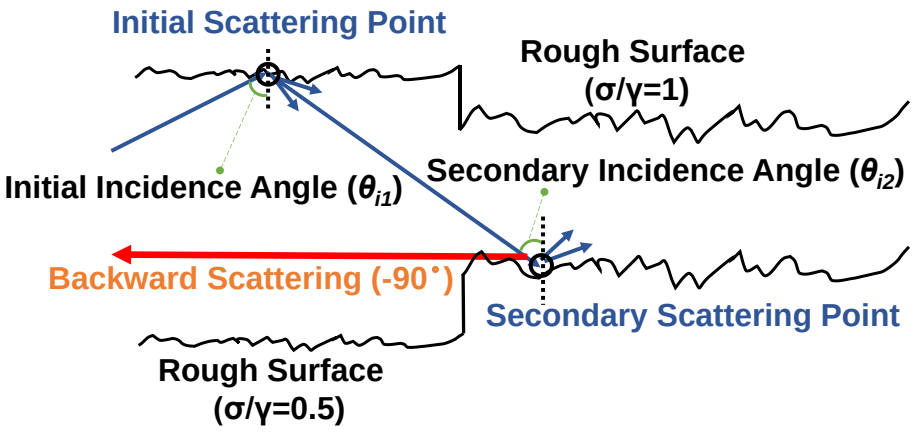

Fig. 10. Scattering in a conventional grooved CLS structure with different levels of surface roughness.

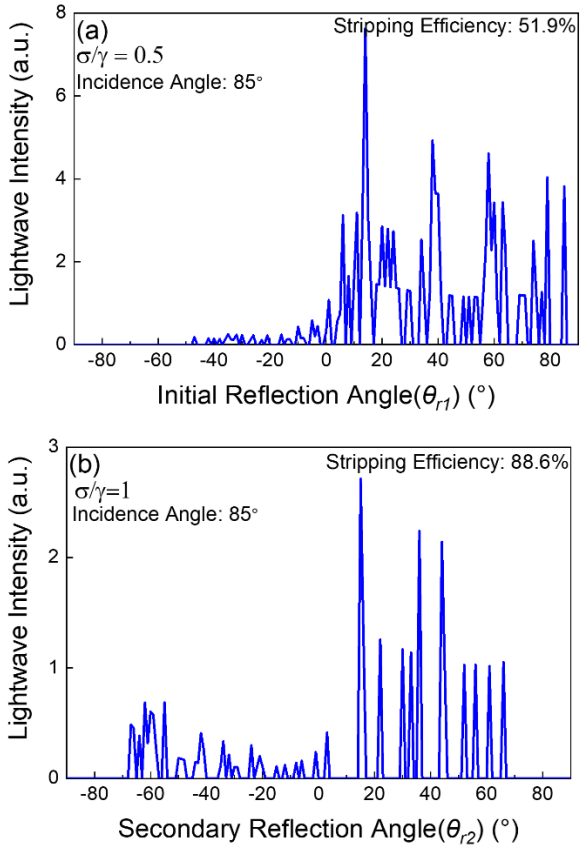

Fig. 11. Calculated light wave intensity distribution as a function of the (a) initial reflection angle (θ_{r1}) under an initial incident angle of 85° with σ/γ=0.5, and (b) secondary reflection angle (θ_{r2}) under a secondary incident angle of 85° with σ/γ=1.

In order to quantitatively analyze the backscattering that occurs in the structure presented in Fig. 9, we calculate the lightwave intensity distribution as a function of the secondary reflection angle (θ_{r2}) under secondary incident angles (θ_{i2}) (Fig. 12) ranging from 0˚ to 80˚ at intervals of 10˚. Interestingly, the amount of forward scattered and backscattered lightwaves is similar in all cases. It should be noted that the backward scattered lightwaves propagate in the direction with a secondary reflection angle of nearly −90˚, which is detrimental to high-power fiber laser oscillators and amplifiers because they cannot be stripped away and can damage fiber laser systems. According to our calculation results, it can be tentatively concluded that CLSs based on the structure in Fig. 10 would suffer from the harmful effects of backscattering.

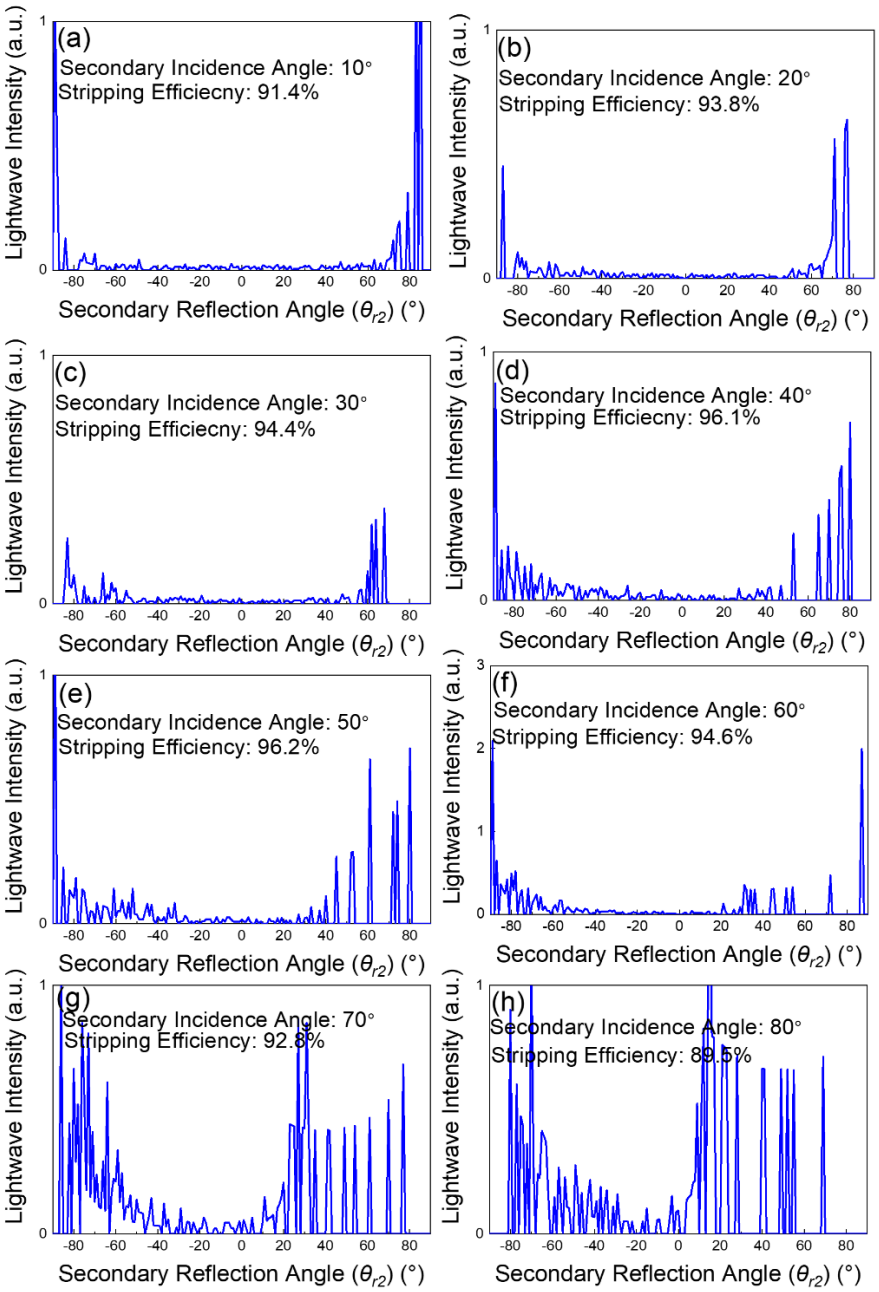

Fig. 12. Calculated lightwave intensity distribution as a function of the secondary reflection angle (θ_{r2}) under secondary incident angles (θ_{i2}) of (a) 10˚, (b) 20˚, (c) 30˚, (d) 40˚, (e) 50˚, (f) 60˚, (g) 70˚, and (h) 80˚.

Fig. 13 presents the calculated lightwave stripping efficiency as a function of the secondary incidence angle (θ_{i2}). The highest stripping efficiency is observed at ~45˚. Although the stripping efficiency for a rough surface of σ/γ=1 is higher than 90%, the total backward scattered light remains considerable.

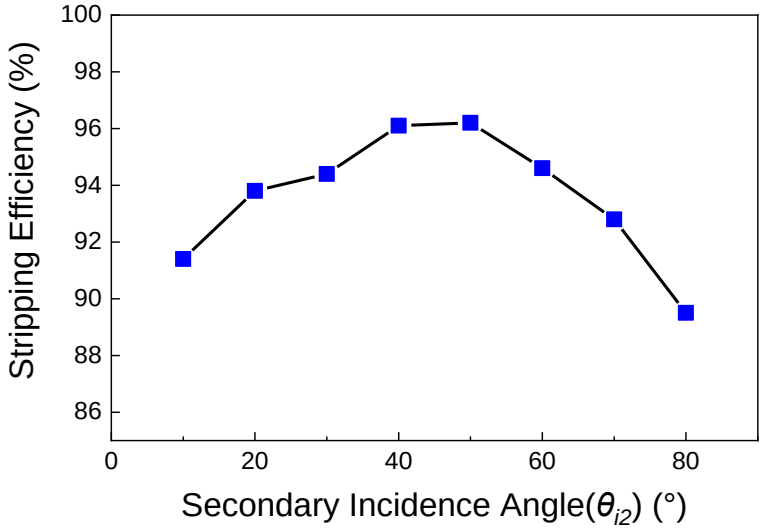

Fig. 13. Calculated light wave stripping efficiency as a function of the secondary incidence angle (θ_{i2}) after striking rough surface at σ/γ=1.

3. Our Proposed CLS structure to suppress Backward scattering

Based on the calculation results, it can be inferred that a structure that combines a section with an unetched smooth surface with a section with a grooved rough surface would suppress backscattering (Fig. 14). Backscattering cannot occur on the smooth surface of the unetched section, with only those lightwaves that violate the TIR condition escaping from the smooth surface. In other words, lightwaves with incidence angles smaller than 80˚ are stripped from the unetched section. This indicates that backscattering in the cascaded grooved section is substantially lower. It should be noted that the unetched region is essential for the gradual stripping of cladding lightwaves as well as the suppression of backscattering.

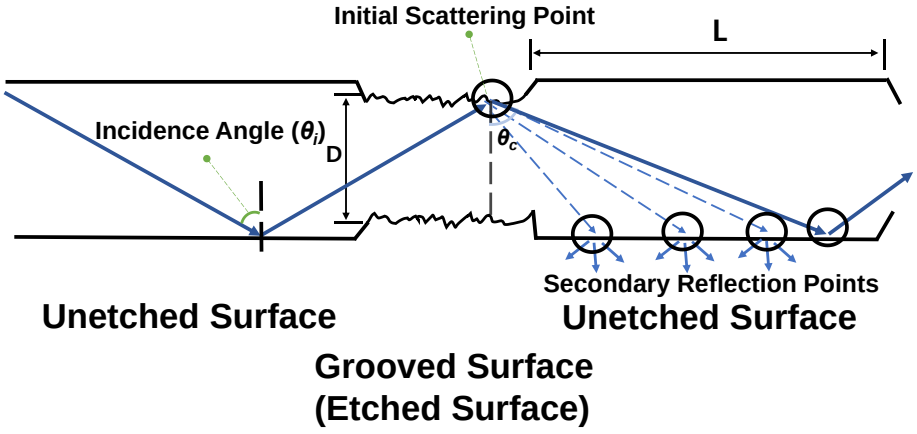

Fig. 14. Structure of the proposed CLS combining grooved and unetched regions.

With the calculation results, the total power of back-scattered light after secondary scattering

in the conventional (Fig. 10) and our proposed (Fig. 14) CLS structures can be estimated. The power of the back-scattered light in the range of - 90 ˚ to 0 ˚ was estimated at ~4.77 % relative to the input beam power in the conventional structure, while it was ~2.43 % in our proposed structure. Note that the back-scattered light in the range from -90˚ to -78.5˚, which is detrimental for high-power laser systems, was ~2.34 % in the conventional structure, whereas almost zero back-scattered light was observed in our proposed structure.

In order to determine the appropriate length of the unetched section, the diameter of the grooved fiber section (D) and the critical angle for TIR (θ_C) need to be considered. For high-power Yb^{3+}-doped fiber amplifiers, the typical diameter for a double-clad fiber is 400 μm, and the critical angle is about 80˚. The lightwaves that are scattered at the secondary scattering point with an angle between 0˚ and 80˚ (the dotted line in Fig. 14) can be eliminated because they cannot meet the TIR condition. Thus, the length ($L_{unetched}$) of the unetched region required to remove all of the lightwave components with a scattering angle of 0˚−80˚ can be calculated as follows:

$$L_{unetched} = tan(\theta_C) \times D = tan(80^{\circ}) \times 400\ (\mu m) = \sim 2.26\ mm \quad (5)$$

Fig. 15 presents the lightwave intensity distribution as a function of the secondary reflection angle (θ_{r2}). Interestingly, more than 90% of the lightwaves are scattered in the forward direction, compared to a minor proportion in the backward direction. Fig. 16 displays the proportion of backscattered lightwaves as a function of θ_{r2}. The proportion of backward-scattered lightwaves decreases as θ_{r2} increases from 80˚ to 90˚, with the maximum backscattering observed at a θ_{r2} of 80˚. From these results, it can be tentatively concluded that our proposed combined structure that alternates sections with an unetched smooth surface with sections with a grooved rough surface is more advantageous than the conventional structure presented in Fig. 10.

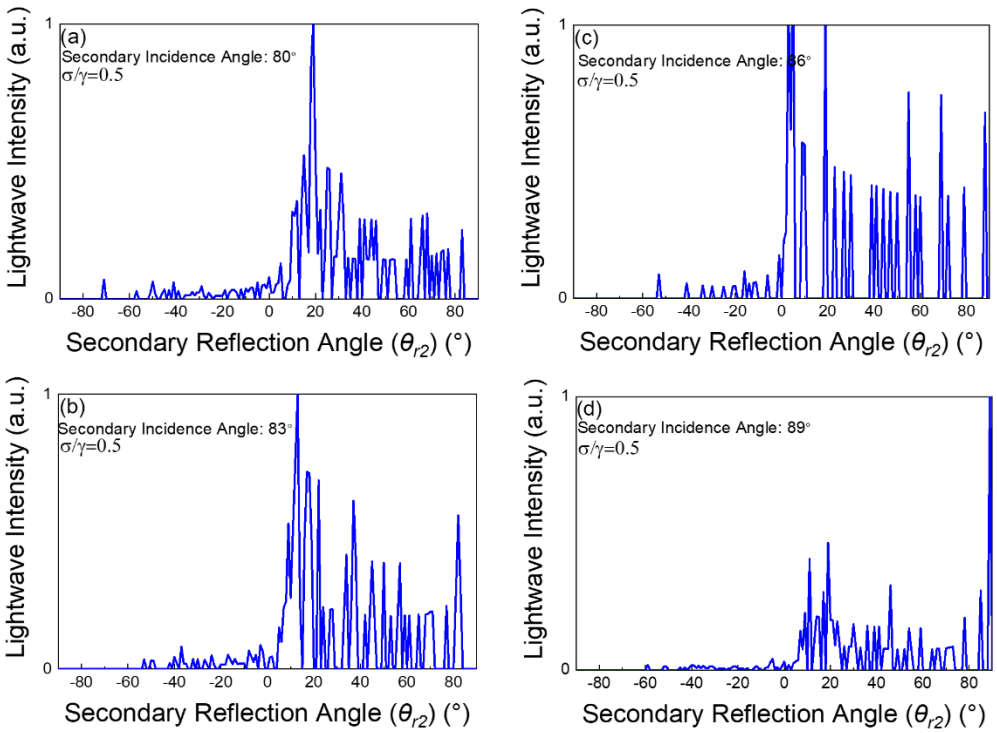

Fig. 15. Calculated lightwave intensity distribution as a function of the secondary reflection angle (θ_{r2}) under second incident angles (θ_{i2}) of (a) 80˚, (b) 83˚, (c) 86˚, and (d) 89˚.

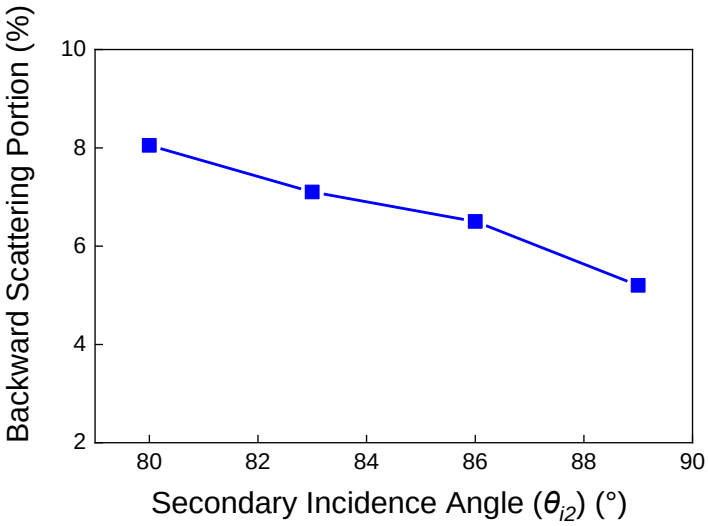

Fig. 16. Calculated proportion of backscattered light waves as a function of the secondary reflection angle (θ_{r2}) for a CLS combining grooved and unetched regions.

4. Experimental Performance Comparison between our proposed structure and an exemplary conventional structure

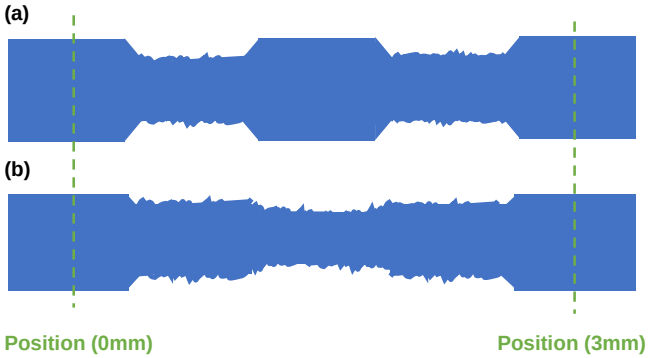

Fig. 17. Schematic of (a) our proposed CLS structure and (b) the representative conventional structure from Refs. [14, 17, 18, 20].

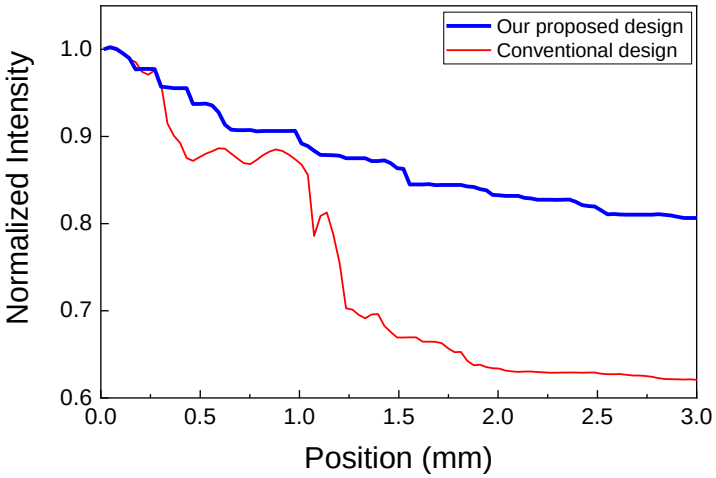

Fig. 18. Calculated residual light intensity distribution for (a) our proposed CLS design and (b) the conventional design from Refs. [14, 17, 18, 20].

In order to verify the effectiveness of our proposed CLS structure, we experimentally compare the lightwave stripping performance of our proposed structure with that of a representative conventional approach (Fig. 17). Our proposed CLS structure alternates unetched and grooved sections, whereas the conventional structure has no unetched region. The conventional structure is assumed to have a tapered section with a rough surface [14, 17, 18, 20]. The residual light intensity distribution along the length of the CLS for both cases is shown in Fig. 18. Our proposed structure was observed to strip lightwaves more gradually than the conventional structure. Our proposed structure (Fig.17(a)) exhibited a stripping efficiency lower than the conventional structure (Fig. 17(b)). The stripping efficiency (η) of our proposed structure was ~89 %, while it was ~97.4 % in the conventional structure.

To further confirm the effectiveness of our proposed CLS structure, we experimentally fabricate the two CLS structures using FG125LA optical fibers and chemical wet etching. Details of this chemical wet etching technique for optical fibers are available in Ref. [27]. The measured scanning electron microscope (SEM) images of the etched surface of our proposed CLS is shown in Fig. 19(a). Evidently, the surface roughness is non-negligible. In this experiment, we use a multimode 60-W laser diode beam at 976 nm to assess the performance of the two CLS structures. The intensity distribution of the stripped lightwaves is indirectly estimated by measuring the temperature distribution along the length of the CLS. In order to measure the thermal images together with temperature distributions, we used a thermal camera (FLIR A310). The camera composed of 16-bit 320 × 240 pixels has a thermal resolution of ≤ 0.05°C, and its length of a smallest pixel box is about 100 μm. We think that the image sensor resolution is sufficient enough to obtain a thermal image of optical fiber.

Fig. 19(b) and (c) presents thermal images for the two CLS structures under the coupled multimode 60-W pump beam, and a comparison of the temperature distribution along the length of the CLS length is displayed in Fig. 19(d). The detecting spectral range of the camera is from 7.5 μm to 13 μm, which is not suitable for detecting a 976-nm laser diode beam. Therefore, we believe that the temperature peaks in Fig. 19(d) are real thermal images of CLSs. The temperature distribution measurements based on thermal images were also conducted in previously demonstrated works on CLSs [3, 6, 9, 12, 14]. It is apparent that our proposed CLS structure achieves mostly uniform lightwave stripping without localized overheating. However, the conventional structure exhibits a strong localized overheating with non-negligible back-scattered light at a position of ~0.5 cm. The temperature peak is believed to be due to back-scattered light, since the fiber end facet was cleaved with an angle of 7˚ to avoid fiber end-facet reflection. Since the back-reflection at the fiber end facet with an angle of 7° would be stripped away in our proposed CLS structure, there would not be an issue of back-reflection at the fiber end facet even in the case of using a fiber with an NA larger than 0.4. Note that a smaller incident angle (for high NA fibers) results in a higher stripping efficiency, as shown in Fig. 5. These experimental results reaffirm that our proposed CLS design with unetched sections is effective in suppressing backscattered light and localized overheating.

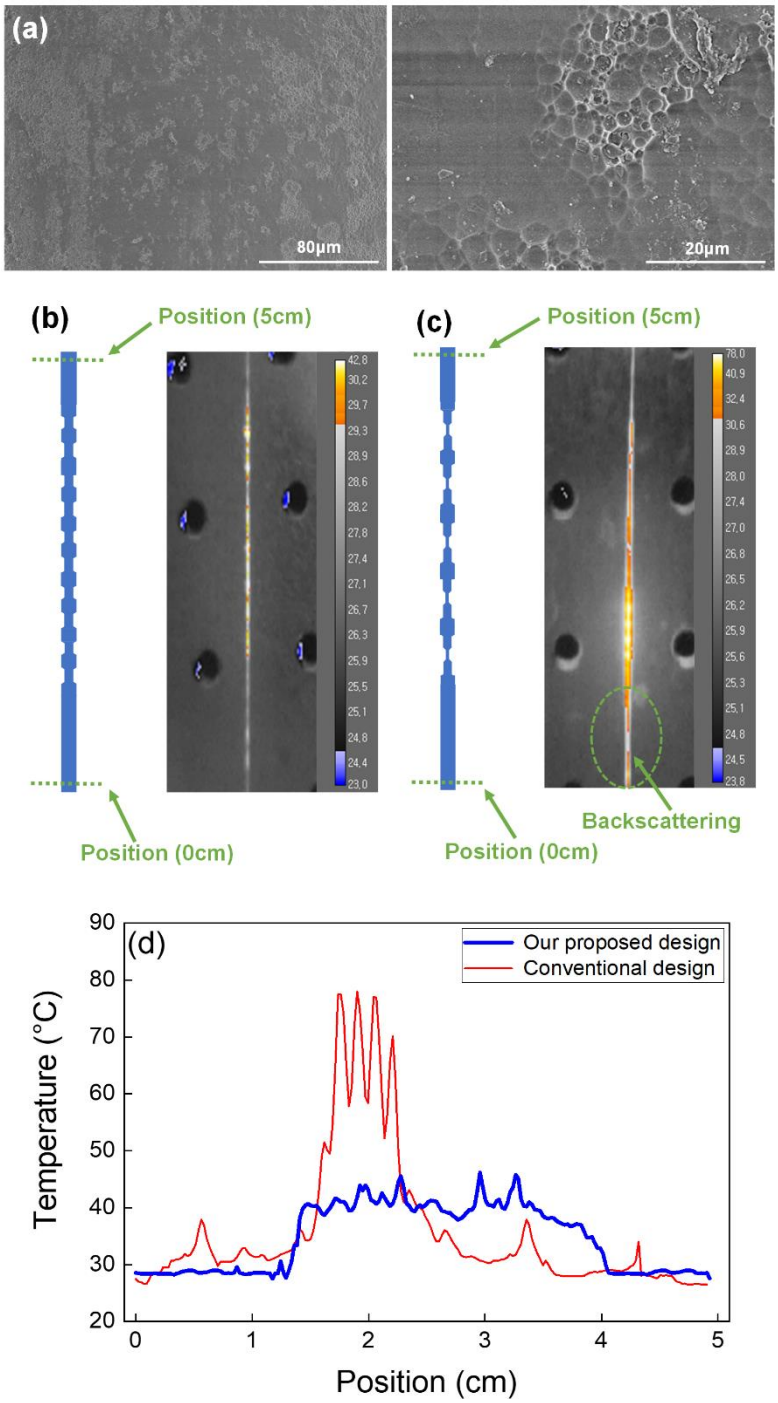

Fig. 19. (a) Measured SEM images of the etched surface of our proposed CLS. Thermal images of (b) our proposed CLS structure and (c) a conventional structure with, a coupled 60-W multimode pump beam. (d) Comparison of the temperature distribution along the length of the CLS for the two structures.

5. Discussion and Future Work

Due to the pandemic situation of COVID19 in South Korea, my research group encountered various difficulties in conducting research for the project. However, we have been making a reasonable progress to achieve the goal. Through this investigation, it was found that the

amount of backscattered cladding light varies significantly with the surface roughness of the grooves. We proposed a periodically grooved CLS structure with multiple unetched sections with an appropriate length and verified its efficacy using numerical simulations and an experiment. The multiple unetched sections were demonstrated to efficiently strip cladding light without localized overheating or backscattering.

We believe that our results provide a useful guideline for the optimal design of high-power CLSs. Our work was focused only on CLSs based on wet etching techniques. For the future, we plan to investigate optimized structures based on CO_2 laser processing in terms of backward scattering.

6. References

[1] C. Jauregui, J. Limpert, and A. Tunnermann, "High-power fibre lasers," *Nature Photon*., vol. 7, pp. 861–867, 2013.

[2] D. J. Richardson, J. Nilsson, and W. A. Clarkson, "High power fiber lasers: current status and future perspectives [Invited]," *J. Opt. Soc. Am. B*, vol.27, pp.B63-B92, 2010.

[3] S. Zou, H. Yu, J. Zhang, J. Zuo, Z. Dong, S. Xu, L. Chang, P. Zhao, and X. Lin., "Highly efficient fiber cladding light stripper fabricated by chemical mask etching method," *J. Lightwave Technol.*, vol. 38, no.18, pp. 5136-5141, 2020.

[4] C. Jauregui, C. Stihler, A. Tünnermann, and J. Limpert, "Origin and evolution of phase-shifts in high-power fiber laser systems: detailed insights into TMI," *Proc. SPIE 10897, Fiber Lasers XVI: Technology and Systems*, 1089704, March 2019.

[5] P. Yan, J. Sun, Y. Huang, D. Li, X. Wang, Q. Xiao, and M. Gong, "Kilowatt-level cladding light stripper for high-power fiber laser," *Appl. Opt.*, vol.56, pp.1935–1939, 2017.

[6] Babazadeh, R. R. Nasirabad, A. Norouzey, K. Hejaz, R. Poozesh, A. Heidariazar, A. H. Golshan, A. Roohforouz, S. N. T. Jafari, and M. Lafouti, " Robust cladding light stripper for high-power fiber lasers using soft metals," *Appl. Opt*., vol.53, pp.2611–2615, 2014.

[7] L. Bansal, V. R. Supradeepa, T. Kremp, S. Sullivan, and C. Headley, "High power cladding mode stripper," *Proc. SPIE 9344, Fiber Lasers XII: Technology, Systems, and Applications*, 93440F, March 2015.

[8] Wetter, M. Faucher, and B. Sévigny, "High power cladding light strippers," *Proc. SPIE 6873, Fiber Lasers V: Technology, Systems, and Applications*, 687327, February 2008.

[9] R. Poozesh, A. Norouzy, A. H. Golshan, A. Roohforouz, A. Babazadeh, R. R. Nasirabad, N. T. Jafari, A. Heidariazar, K. Hejaz, A. Alavian, and A. Amidian, "A novel method for stripping cladding lights in high power fiber lasers and amplifiers," *J. Lightwave Technol*., vol.30, pp.3199–3202, 2012.

[10] Kliner, K.-C. Hou, M. Plötner, C. Hupel, T. Stelzner, T. Schreiber, R. Eberhardt, and A. Tünnermann, "Fabrication and evaluation of a 500W cladding-light stripper," *Proc. SPIE 8616*, MOEMS and Miniaturized Systems XII, 86160N, March 2013.

[11] H. An, X. Liu, and Z. Bi, "Study and design of cladding power stripper for high power fiber laser systems," *High Power Laser Sci. Eng*., vol.4, e28, 2016.

[12] W. Guo, Z. Chen, H. Zhou, J. Li, and J. Hou, "Cascaded cladding light extracting strippers for high power fiber lasers and amplifiers," *IEEE Photon. J*., vol.6, pp.1–6, 2014.

[13] M. Wysmolek, T. Theeg, H. Sayinc, J. Neumann, and D. Kracht, "All-fibre high power pump stripper manufactured by CO_2 laser microstructuring," *SPIE Photonics West: LASE2.-7*, 2013

[14] E. Yildirim, A. Karatutlu, E. Balk, Y. Midilli, and B. Ortac, "Combined method for the fabrication of high-power cladding light stripper using a buffered oxide etchant," *Appl. Opt*., vol.58, pp.6926-6933, 2019.

[15] M. Wysmolek, C. Ottenhues, T. Pulzer, T. Theeg, H. Sayinc, M. Steinke, U. Morgner, J. Neumann, and D. Kracht, "Microstructured fiber cladding light stripper for kilowatt-class laser systems," *Appl. Opt*., vol.57, pp.6640–6644, 2018.

[16] Adam, I. Kiyat, and S. K. Kalyoncu, "Practical, rapid, and process-on-place polymer-free cladding power stripping for high power fiber lasers," *Appl. Opt*., vol.59, pp.2725-2730, 2020.

[17] S. Zou, H. Chen, J. Zhang, H. Yu, Z. Zhang, J. Sun, X. Lin, "Cladding light stripper of high average stripped power density with high attenuation of 39 dB and low temperature rise," *IEEE. Photon. J*., vol.10, 7100610, 2018.

[18] M.-J. Yan, Z. Wang, L.-Q. Meng, L. Yin, Z.-G. Han, H. Shen, H.-L. Wang, and R.-H. Zhu, "Heat suppression of the fiber coating on a cladding light stripper in high-power fiber laser," *Appl. Opt*., vol. 57, no. 3, pp. 485–491, 2018.

[19] K. Boyd, N. Simakov, A. Hemming, J. Daniel, R. Swain, E. Mies, S. Rees, W. A. Clarkson, and J. Haub, "CO_2 laser-fabricated cladding light strippers for high-power fiber lasers and amplifiers," *Appl. Opt.*, vol.55, pp.2915–2920, 2016.
[20] L. Yin, M. Yan, Z. Han, H. Wang, H. Shen, and R. Zhu, "High power cladding light stripper using segmented corrosion method: theoretical and experimental studies," *Opt. Express*, vol.25, pp.8760–8776, 2017.
[21] S. Boehme, K. Hirte, S. Fabian, C. Hupel, T. Schreiber, R. Eberhardt, and A. Tünnermann, "CO_2 laser-based coating process for high power fiber application," *Proc. SPIE 8968, Laser-based Micro- and Nanoprocessing VIII*, 89680Z, March 2014.
[22] T. Li, J. Wu, Y. Sun, Y. Wang, and Y. Ma, "An improved method for stripping cladding light in high power fiber lasers," *Proc. SPIE 9255, XX International Symposium on High-Power Laser Systems and Applications 2014*, 92550M, February 2015.
[23] D. Bergström, J. Powell, and A. F. H. Kaplan, "A ray-tracing analysis of the absorption of light by smooth and rough metal surfaces," *J. Appl. Phys.*, vol.101, p.113504, 2007.
[24] D. Bergström, J. Powell, and A. F. H. Kaplan, "The absorption of light by rough metal surfaces-A three-dimensional ray-tracing analysis," *J. Appl. Phys.*, vol.103, p.103515, 2008.
[25] Macaskill, "Geometric optics and enhanced backscattering from very rough surfaces," *J. Opt. Soc. Am. A*, vol.8, pp.88–96, 1991.
[26] M. J. Kim, J. C. Dainty, A. T. Friberg, and A. J. Sant, "Experimental study of enhanced backscattering from one-and two dimensional random rough surfaces," *J. Opt. Soc. Am. A*, vol.7, pp.569–577, 1990.
[27] S. Ko, J. Lee, J. Koo, B. Joo, M. Gu, and J. Lee "Chemical Wet Etching of an optical Fiber Using a Hydrogen Fluoride-Free Solution for a Saturable Absorber Based on the Evanescent Field Interaction," *J. Lightwave Technol.*, vol.30, pp.3776–3784, 2016.

- **How were the results disseminated to communities of interest?**

[1] The results of this work have been published as an article in a peer-reviewed journal as following: “Efficient suppression of backward light scattering for optical fiber cladding light stripper,” *Journal of Lightwave Technology*, vol. 40, no. 22, pp. 7412 – 7420, November 15, 2022.

[2] The results of this work will also be presented at a technical conference as following: “Theoretical investigation into backscattering in optical fiber cladding light stripper,” *Advanced Solid State Lasers in Optica Laser Congress and Exhibition*, paper JTu6A.10, Barcelona, December 13, 2022.